Am J Transl Res 2023;15(6):3912-3927
www.ajtr.org /ISSN:1943-8141/AJTR0150315

Original Article

A ferroptosis-related ceRNA network in hepatocellular carcinoma for potential clinical applications

Zelong Yang, Kun He, Weigang Chen, Yong Chen

Department of Hepatobiliary Surgery, The First Affiliated Hospital, Airforce Military Medical University, Xi'an 710032, Shaanxi, China

Received March 23, 2023; Accepted May 3, 2023; Epub June 15, 2023; Published June 30, 2023

Abstract: Objective: To explore the competing endogenous RNA (ceRNA) network related to ferroptosis in hepatocellular carcinoma (HCC) and its promise for clinical application. Methods: We obtained RNA sequencing data for HCC and relevant clinical information from The Cancer Genome Atlas (TCGA) database. To assess the involvement of the autophagy, pyroptosis, and ferroptosis pathways in HCC, we used single-sample Gene Set Enrichment Analysis (ssGSEA) to compute scores for each sample based on pre-defined gene sets. We conducted Weighted Gene Co-Expression Network Analysis (WGCNA) to effectively modularize lncRNA, miRNA, and mRNA. Through extensive correlation analyses, we pinpointed the most crucial ferroptosis-associated modules. Moreover, we utilized online prediction tools to construct a corresponding ceRNA network. To establish the reliability of our results, we randomly chose a ceRNA axis consisting of DNAJC27-AS1/miR-23b-3p/PPIF for experimental validation. We performed luciferase reporter assays to validate the binding sites of DNAJC27-AS1, miR-23b-3p, and PPIF. Results: We found a significant correlation between the level of ferroptosis and the overall survival of patients with HCC. Thus, we constructed a comprehensive ferroptosis-related ceRNA network. Our experimental findings revealed that DNAJC27-AS1 and PPIF act as direct sponges of miR-23b-3p, and thus are capable of downregulating ferroptosis in HCC cells. Conclusion: The ferroptosis-associated ceRNA network presented in this study represents a valuable resource for advancing our understanding of the role of ferroptosis in HCC.

Keywords: Hepatocellular carcinoma, competing endogenous RNA, ferroptosis, WGCNA

Introduction

Hepatocellular carcinoma is the most common type of liver cancer, with a high incidence and mortality rate worldwide [1]. While there are several treatment options available, the success rates for these treatments are still unsatisfactory. The 5-year survival rate for HCC patients, in particular, is only 18% [2]. The need for expanding the therapeutic efficacy for HCC remains unmet.

The strategy of inducing cell death is becoming more popular as an approach to treat cancer, including HCC [3]. Various forms of regulated cell death (RCD) have been shown to have different effects on the progression of HCC [4]. Different types of regulated cell death (RCD) have been found to have varying effects on the progression of HCC. In 2012, Dixon et al. introduced a new form of RCD known as ferroptosis, which is distinguishable from apoptosis both by its morphology and biochemical features [5]. Erastin, a selective inhibitor of cancer cell proliferation, has been shown to trigger ferroptosis in cancer cells [6].

Cystine is an important component for the production of glutathione (GSH), a key regulator of glutathione peroxidase 4 (GPX4) that helps to reduce the levels of intracellular lipid peroxidation. When there is dysfunction in the GPX4 and related genes, accumulation of superoxide can occur. This causes mitochondrial damage and ultimately leads to ferroptosis [7]. Ferroptosis can be induced by various factors, including iron overload [8] and p53 dysregulation [9], and is involved in a range of liver diseases such as hepatic ischemia-reperfusion injury, liver fibrosis, nonalcoholic steatosis, and liver failure [10]. Recent research has also reported the use of inducing ferroptosis as a means of inhibiting

liver cancer cells [11], and targeting ferroptosis may be effective in treating sorafenib-resistant HCC patients [12, 13]. Therefore, a better understanding of the regulatory networks involved in ferroptosis in HCC is crucial.

Competing endogenous RNA (ceRNA) is a sophisticated post-transcriptional regulatory mechanism that involves lncRNA and mRNA competing with miRNA through response elements [14].

The classical lncRNA-miRNA-mRNA ceRNA networks have been widely studied and reported in the progression and pathogenesis of various cancers [15, 16]. In these ceRNA networks, lncRNAs act as miRNA sponges, binding to and inhibiting miRNA activity, which in turn results in increased expression levels of target mRNAs. Non-coding RNA has emerged as a critical regulator of ferroptosis in cancer [17]. For example, the lncRNA NEAT1 was shown to enhance erastin-induced ferroptosis in HCC cells by promoting MIOX expression through competitive binding to miR-362-3p [18]. Additionally, the interaction of P53RRA with G3BP1 can facilitate the transposition of p53 into the nucleus and activate cell-cycle arrest, apoptosis, and ferroptosis [19]. These findings highlight the therapeutic value of ceRNA for manipulating ferroptosis for cancer treatment.

In this study, we used data from the TCGA database to investigate the complex interplay between ferroptosis and HCC. We analyzed clinical and RNA expression data through ssGSEA scoring and WGCNA analysis, which allowed us to identify mRNAs, lncRNAs, and miRNAs implicated in the regulation of ferroptosis. Using multiple online tools, we were able to predict the lncRNA and mRNA targets of the ferroptosis-associated miRNAs, and further construct a ceRNA network based on hub miRNAs. Finally, we validated one ceRNA axis in the network. Overall, our study lays the groundwork for future research into the intricate regulatory mechanisms of ferroptosis in the context of HCC.

Methods

Data collection

The RNA sequencing data, along with associated clinical data, comprising 374 HCC samples and 50 adjacent samples, were acquired from the TGCA database (http://portal.gdc.cancer.gov/repository). The autophagy-related gene set was obtained from the Human Autophagy Database (http://www.autophagy.lu/index.html), while the gene sets associated with ferroptosis and pyroptosis were summarized from previously published studies [20, 21].

Identification of ferroptosis as the target analysis gene sets

The "limma" package was used to analyze differentially expressed gene sets related to ferroptosis, autophagy, and pyroptosis. A cut-off value was established, with the absolute value of log fold change ($|\log FC|$) set to be greater than or equal to 1.5 with a *P*-value less than 0.05. Subsequently, the "GSVA" R package was used to employ ssGSEA and obtain the enrichment scores of the gene sets related to ferroptosis, autophagy, and pyroptosis. The "survival" R package was then used to compare the survival differences of the ssGSEA scores of the different gene sets based on the median cutoff value. Following analysis, the ferroptosis-associated gene set was identified for further exploration through survival analysis.

Analysis of co-expression module construction of HCC

The co-expression analysis was conducted using the mRNA, lncRNA, and miRNA expression data with the "WGCNA" package. The independence and average connectivity degree of different modules were tested using the gradient method, and power values ranging from 1 to 30 were used. The appropriate power value was determined when the degree of independence reached 0.8. The correlation between each co-expression module and ferroptosis-related ssGSEA scores was calculated, and the module genes with the strongest correlation were selected for construction of the ceRNA network.

LncRNA-miRNA-mRNA network construction

To construct a lncRNA-miRNA-mRNA network, several steps were taken. First, miRNA-mRNA and miRNA-lncRNA interactions were predicted through various databases including miRmap [22], miRanda [23], miRDB [24], TargetScan [25], miRTarBase [26], miRcode [27], and

Table 1. Sequence information of siRNA for study genes

Gene	Sense (5'-3')	Antisense (5'-3')
DNAJC27-AS1 siRNA1	GUGCCUCCAUAGUCAUUAUTT	AUAAUGACUAUGGAGGCACTT
DNAJC27-AS1 siRNA2	GGAGCAGGGUGGAAAUUAATT	UUAAUUUCCACCCUGCUCCTT
DNAJC27-AS1 siRNA3	GGCUCAGUUUCCUUAUAUATT	UAUAUAAGGAAACUGAGCCTT
PPIF siRNA1	CUGACGAGAACUUUACACUTT	AGUGUAAAGUUCUCGUCAGTT
PPIF siRNA2	CAAGCAUGUUGUGUUCGGUTT	ACCGAACACAACAUGCUUGTT
PPIF siRNA3	CAUCCAAGAAGAUUGUCAUTT	AUGACAAUCUUCUUGGAUGTT

Table 2. Sequences of primers used for amplification of target genes

Gene	Primer sequence (5'-3')
PPIF-F	CGCTTTCCTGACGAGAACTTT
PPIF-R	TCTTTGACGTGACCGAACACA
DNAJC27AS1-F	GAGAGTCCGTGTGAGAACCG
DNAJC27AS1-R	CCACCCACACTCTGAAGGAC
miR-23b-3p-RT	GTCGTATCCAGTGCAGGGTCCGAGGTATTCGCACTGGATACGACGTGGTA
miR-23b-3p-F	GCTAATCACATTGCCAGGGAT
GAPDH-F	GGAGCGAGATCCCTCCAAAAT
GAPDH-R	GGCTGTTGTCATACTTCTCATGG
U6-2Q-F	CTCGCTTCGGCAGCACA
U6-2Q-R	AACGCTTCACGAATTTGCGT
Universal R (URP) Long A	GTGCAGGGTCCGAGGT

F: Forward, R: Reverse.

STRBase [28]. Secondly, both the lncRNAs and mRNAs were identified by negatively co-expressing them with one same miRNA. Finally, the identified lncRNAs, mRNAs, and miRNAs were intersected to identify candidates for network construction. The ceRNA regulatory network was visualized using Cytoscape 3.8.1.

Cell lines and cell transfection

HepG2 cells, BEL7402 cells, Hep2b, and HuH7 cells were obtained from the American Type Culture Collection (ATCC) and cultured in Dulbecco's Modified Eagle Medium (DMEM) supplemented with 10% fetal bovine serum (FBS) from Hyclone, 100 U/mL of penicillin from Gibco, and 0.1 mg/mL of streptomycin from Gibco. The cells were maintained at 37°C in a humidified atmosphere of 95% O_2 and 5% CO_2.

The overexpression plasmids and siRNAs of DNAJC27-AS1, PPIF, and inhibitors of miR508-3p were provided by GenePharma Co., Ltd. (Shanghai, China). The overexpression plasmid vector used was a pEX-3 vector, while the siRNA sequences for DNAJC27-AS1 and PPIF can be found in **Table 1**. Cells were transfected with varying siRNAs in MEM medium using 90 nM of each siRNA duplex or with 0.8 ug of different plasmids using Lipofectamine 2000 transfection reagent (Thermo Fisher Scientific, Inc., USA) according to the manufacturer's instructions. After 48 h of transfection, cells were harvested for further experiments.

Fluorescence quantitative real-time PCR

Quantitative RT-PCR was carried out according to the manufacturer's instructions. First, total RNA was isolated using the TRIpure Reagent (RP1001, Bioteke Co., Ltd., Beijing, China), and reverse transcription was performed on 1 μg of RNA using the BeyoRT II M-MLV kit (D7160L, Beyotime, Shanghai, China). The resulting cDNAs were then used for semi-quantitative PCR using 2×Taq PCR MasterMix (PC1150, Solarbio Life Science Co., Ltd., Beijing, China) and SYBR Green (SY1020, Solarbio Life Science Co., Ltd.). The qPCR instrument (LightCycler®480 II, Roche, Switzerland) was used to amplify the samples, and fluorescence was measured after each extension step. Melting curves were used to confirm the specificity of the PCR products. Finally, the $2^{-\Delta\Delta CT}$ method was employed for data analysis. Specific primer sets for each gene are detailed in **Table 2**.

Luciferase reporter assay

Based on the mentioned predictions, the wild-type (wt) binding site sequence was amplified by PCR and cloned into a dual-luciferase reporter vector, pmirGLO. A site-directed mutation (mut) was also created at the possible target site of the target gene. The obtained recombinant plasmids were co-transfected with miR-23b-3p mimics into logarithmically growing 293T cells. Two experimental groups were created, with the first group consisting of pmirGLO-wtDNAJC27-AS1+NC mimics, pmirGLO-mutDNAJC27-AS1+NC mimics, pmirGLO-wtDNAJC27-AS1+miR-23b-3p mimics, and pmirGLO-mutDNAJC27-AS1+miR-23b-3p mimics. The second group consisted of pmirGLO-PPIF-wtUTR+NC mimics, pmirGLO-PPIF-mutUTR+NC mimics, pmirGLO-PPIF-wtUTR+miR-23b-3p mimics, and pmirGLO-PPIF-mutUTR+miR-23b-3p mimics. After 48 hours, luciferase activity was measured with a multifunction microplate reader (M200Pro, Tecan, Switzerland), and the Dual Luciferase Reporter Gene Assay Kit (cat. no. KGAF040) from KeyGEN BioTECH Co., Ltd. (Jiangsu, China) was used. The control was set as the first group in each experiment.

Western blotting

TP53 antibody (cat. no. PAA928Ra01. Concentration used: 1/800), and PPIF antibody (cat. no. PAB549Hu01. Concentration used: 1/1000) were purchased from Uscn Life Science Inc., Wuhan, China. SLC7A11 antibody (cat. no. ab175186. Concentration used: 1/1000), GPX4 antibody (cat. no. ab40993. Concentration used: 1/1000), and GAPDH antibody (cat. no. ab8245. Concentration used: 1/1000) were purchased from Abcam (Cambridge, UK). HepG2 and BEL7402 cells were collected and rinsed with PBS post-treatment with drugs or genetic modifications. The total cellular protein was extracted using a protein extraction buffer including NaCl, Tris (pH 7.2), EDTA, Triton X-100, glycerol, and SDS. Equal amounts of proteins (50 μg/lane) were separated by 10% SDS-PAGE and transferred onto PVDF membranes. The membranes were then immunoblotted with primary antibodies, followed by incubation with peroxidase-conjugated goat anti-mouse or anti-rabbit secondary antibodies. Staining was conducted using an enhanced chemiluminescence system, and image acquisition was conducted using a scanner (CanoScan 5600F, Tokyo, Japan).

Reactive oxygen species (ROS) and mitochondrial membrane potential detection

The Cellular ROS Assay Kit (cat. no. ab113851, Abcam) and Novocyte Flow Cytometer (ACEA, Bioscience, USA) were employed to quantify the levels of ROS in cells. The JC-1 assay kit (cat. no. M8650, Solarbio Life Science Co., Ltd.) was used to measure the mitochondrial membrane potential of the cells and flow cytometry analysis with excitation set to 488 nm was used for detection. All steps were strictly in accordance with the instructions.

Cell viability and GSH assay

The Cell Counting Kit-8 (CCK-8) (cat. no. CK04. Dojindo Laboratories, Kumamoto, Japan) was utilized to detect the cell viability. To detect GSH levels, a GSH ELISA kit (cat. no. CEA294Ge, Uscn Life Science Inc.) was employed. All steps were strictly in accordance with the instructions.

Statistical analysis

Statistical analysis of the data was performed using GraphPad Prism 8 software (GraphPad, Inc., San Diego, CA, USA). Normally distributed data were presented as mean ± standard deviation and compared using Student's t-test for two groups or one-way analysis of variance (ANOVA) for multiple groups. Post-hoc analysis was conducted using Tukey's multiple comparison test, and *P* values were corrected using the Bonferroni method. Non-normally distributed data were presented as median and interquartile range and analyzed using non-parametric tests. Spearman's correlation analysis was performed to test the correlation between variables. All statistical analyses were two-sided, and $P<0.05$ or less than the adjusted value was considered significant.

Results

Ferroptosis was associated with the overall survival of HCC patients

The flowchart depicting the methodology utilized in this study is presented in **Figure 1**. Initially, ssGSEA was conducted to determine

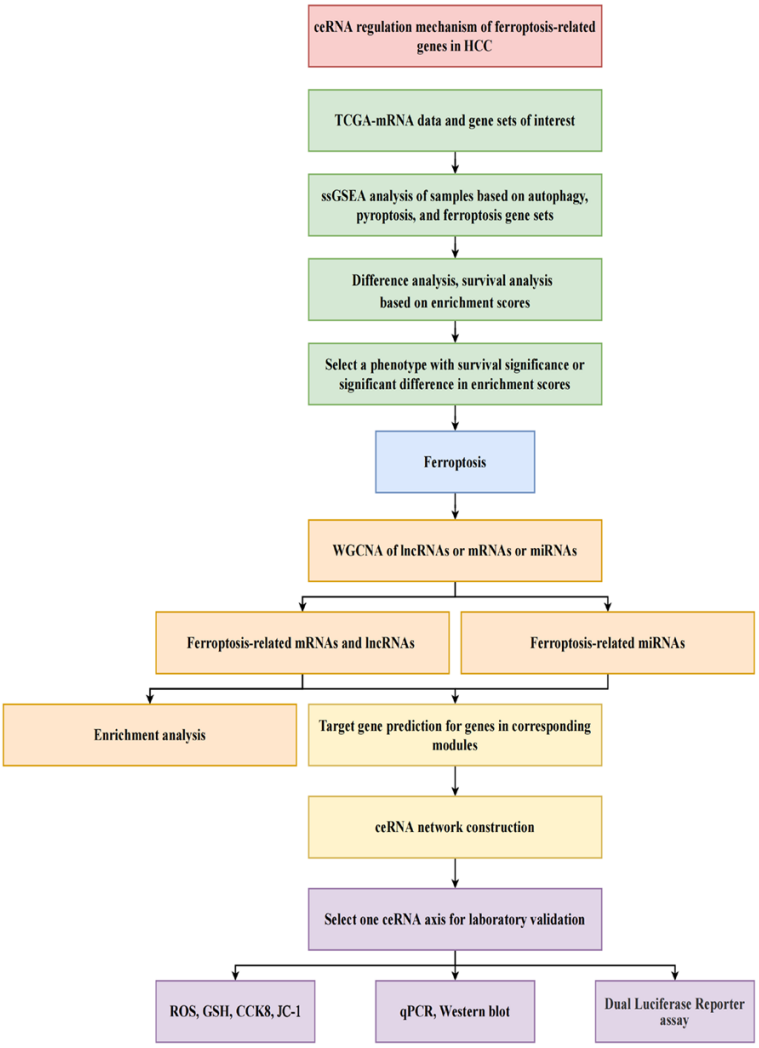

Figure 1. Flow chart in this study.

the expression levels of genes associated with pyroptosis, autophagy, and ferroptosis for each sample. Further, the enrichment scores of the genes were analyzed and depicted by a heat map and boxplot, as shown in **Figure 2A** and **2B**. Subsequently, a comparative analysis of the enrichment scores between cancerous and non-cancerous tissues was performed. It was observed that while the ferroptosis-related enrichment scores remained unchanged, there was a significant difference in the pyroptosis and autophagy-related scores between the two tissues, as depicted in **Figure 2C**. Moreover, Kaplan-Meier survival analysis was conducted to find a correlation between these enrichment scores and patient prognosis. Strikingly, patients with higher ferroptosis-related scores exhibited poorer prognosis (P=0.018), as illustrated in **Figure 2D-F**.

Identification of ferroptosis-associated genes using WGCNA

The analysis showed that the WGCNA reached a scale independence value of 0.805, ensuring a relatively high-average connectivity (**Figure 3A**). Following the construction of a clustering tree and the division of mRNA genes into different modules, correlation analysis was conducted between gene expression in each module and ferroptosis-related ssGSEA scores. The genes in the royal blue and salmon modules had the most positive correlation, while the grey module had the most negative correlation, with the enrichment scores (**Figure 3B**, **3C**). In the WGCNA analysis of lncRNAs, the genes in the dark green and dark red modules had the most positive correlation, while the genes in the blue module had the most negative correlation with the enrichment scores (**Figure 3D-F**). Additionally, the miRNAs in the turquoise module had the most positive correlation, while the miRNAs in the red module had the most negative correlation with the enrichment scores (**Figure 3G-I**). Overall, these findings suggest that the different modules and their respective genes and miRNAs play important roles in regulating ferroptosis.

The construction of a ceRNA network related to ferroptosis in HCC

After utilizing several bioinformatic tools to predict the miRNA-mRNA and miRNA-lncRNA interactions within the modules that had the strongest correlation with ferroptosis enrichment scores, we identified a total of 652 pairs of miRNAs that positively correlated with ferroptosis

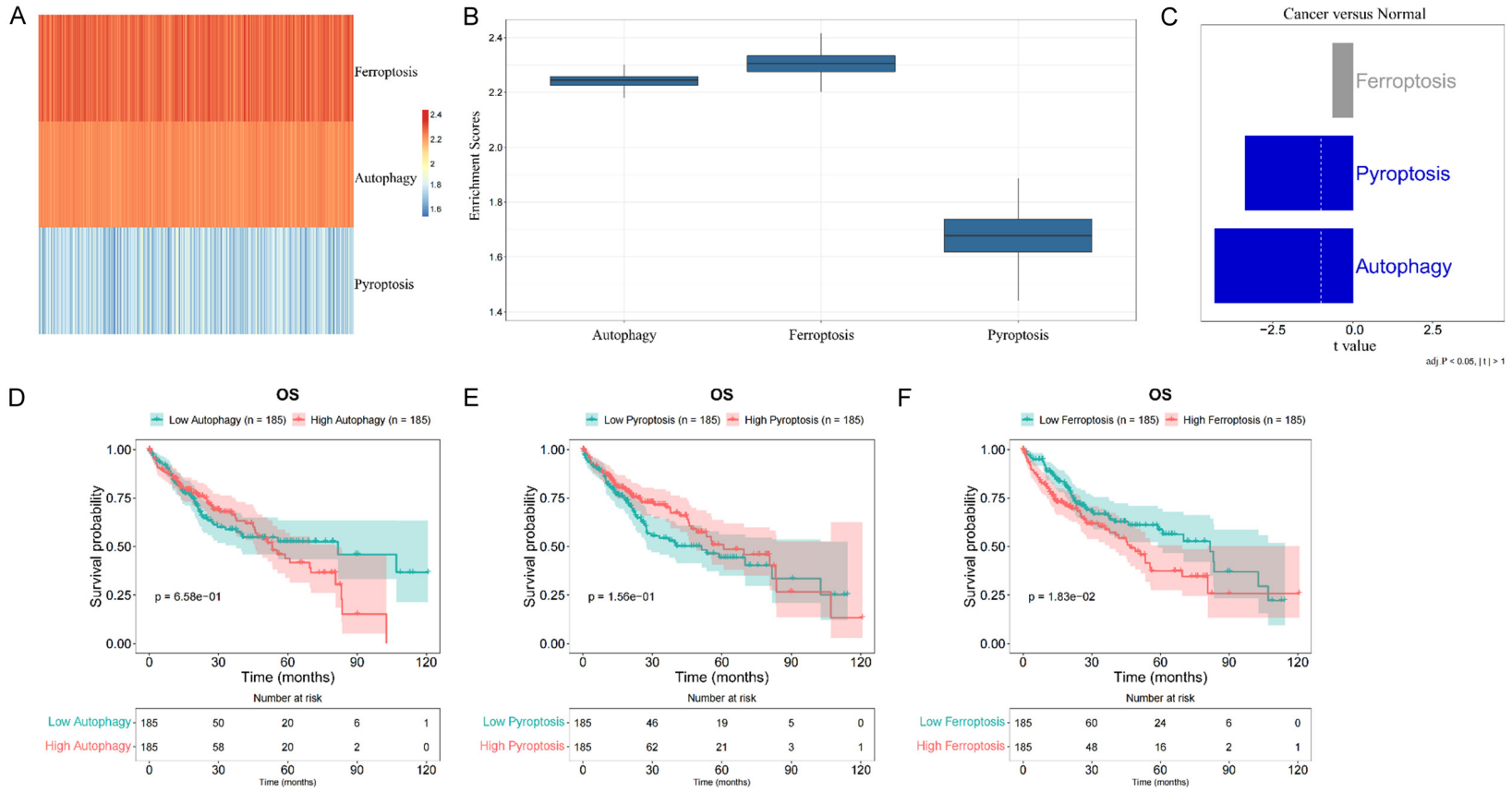

Figure 2. Differential analysis and survival analysis of ssGSEA scores related to ferroptosis, autophagy, and pyroptosis. A. Heatmap of ssGSEA scores for the three phenotypes. B. Boxplots of ssGSEA scores for the three phenotypes. C. Differential analysis of ssGSEA scores for the three phenotypes. D. Kaplan-Meier survival analysis of ssGSEA scores for autophagy. E. Kaplan-Meier survival analysis of ssGSEA scores for pyroptosis. F. Kaplan-Meier survival analysis of ssGSEA scores for ferroptosis.

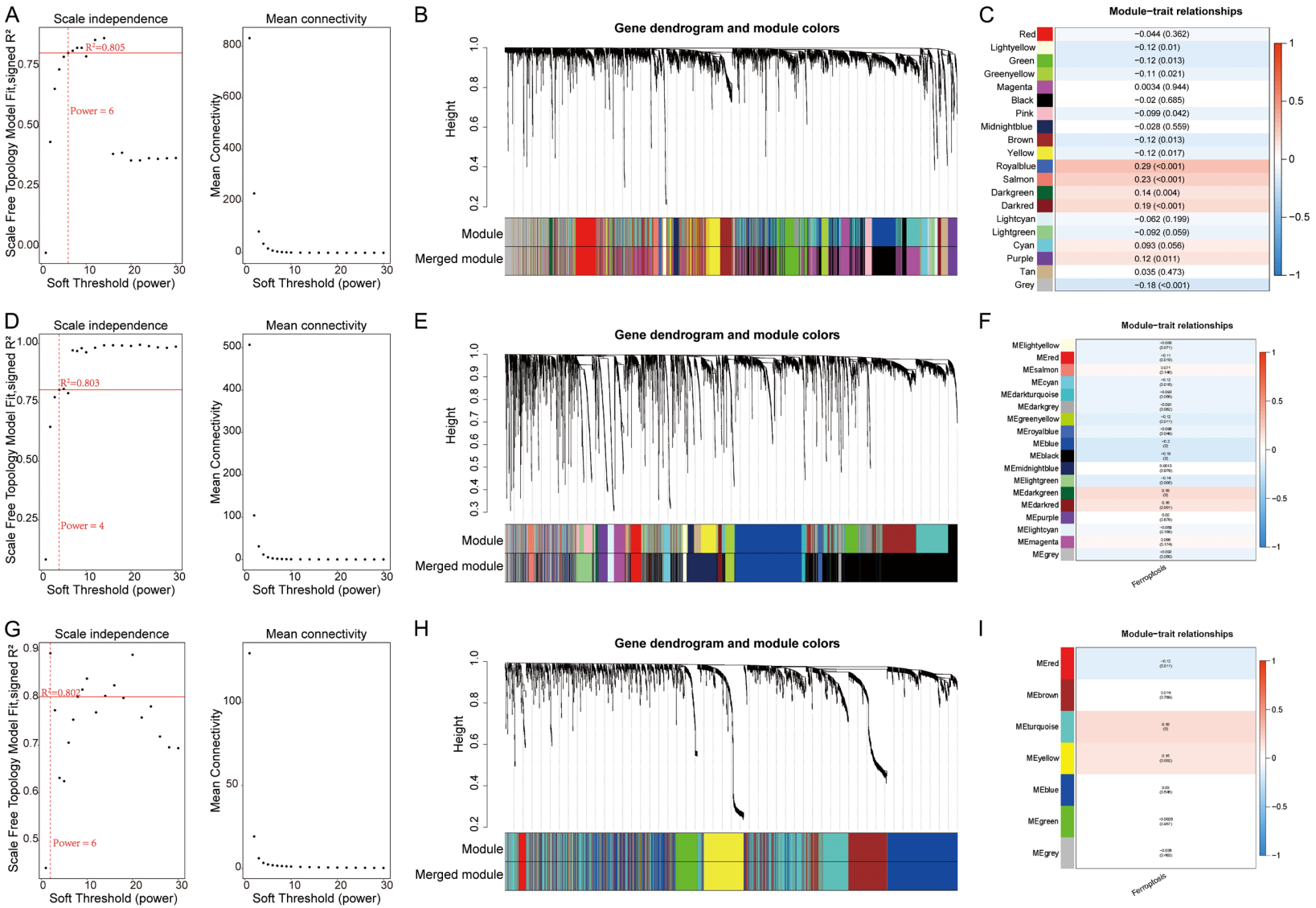

Figure 3. Analysis of network topology for various soft-thresholding powers, clustering dendrograms for the three types of genes, and heatmap for the relationships of the module trait. A. In the WGCNA analysis of mRNA, the soft-thresholding power was set to 6. B. A total of 20 mRNA co-expression modules were constructed and shown in different colors. C. Each color corresponds to a module eigengene of mRNA; each cell contains the corresponding ferroptosis correlation and *P*-value. D-F. In the WGCNA analysis of lncRNA, the soft-thresholding power was set to 4, a total of 18 mRNA co-expression modules were constructed, and the corresponding correlation between modules and ferroptosis is shown. G-I. The WGCNA analysis of miRNA.

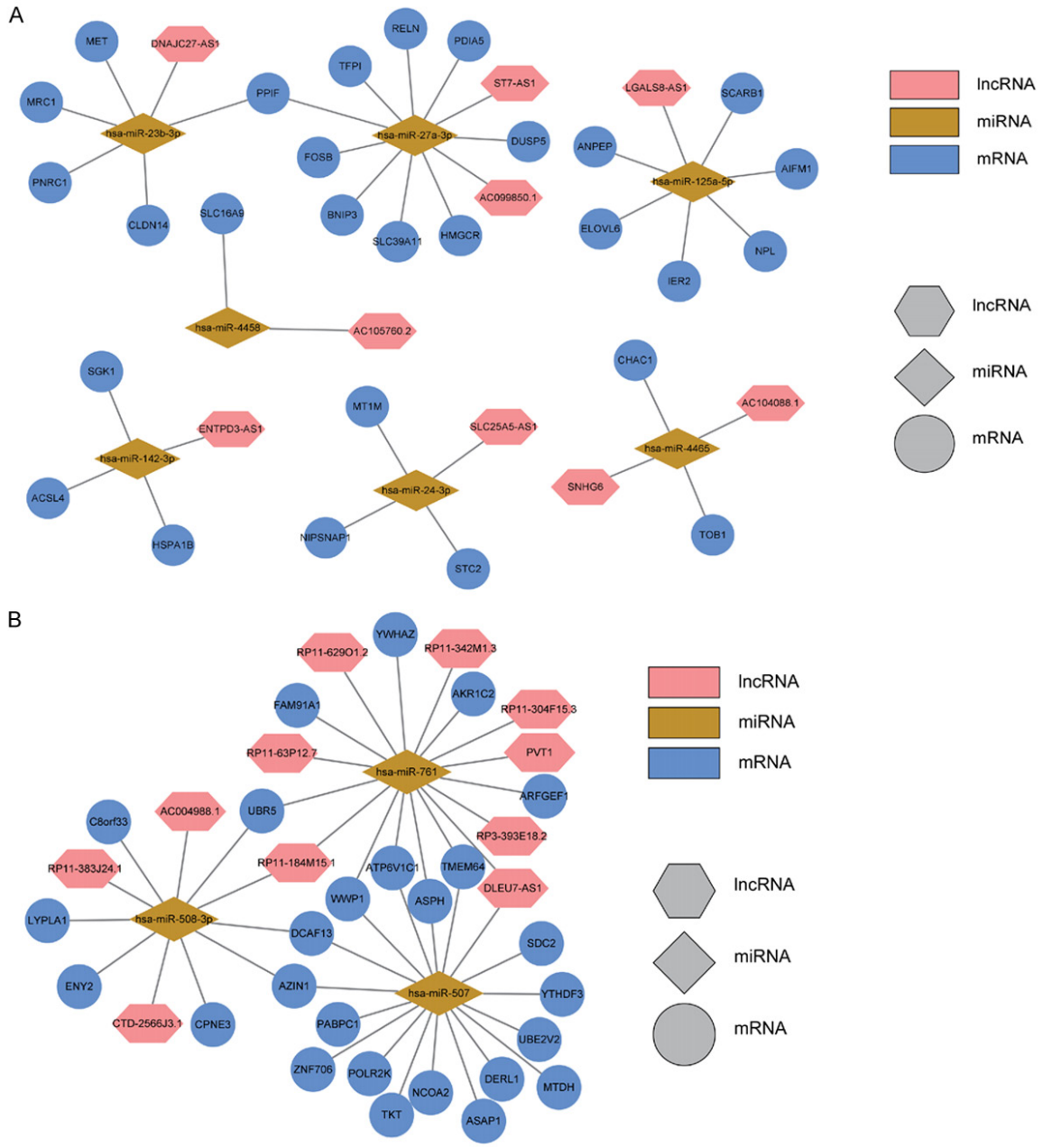

Figure 4. ceRNA network construction. A. The ceRNA network consists of the negative ferroptosis-related lncRNAs and mRNAs and the positive ferroptosis-related miRNAs. B. The ceRNA network consists of the positive ferroptosis-related lncRNAs and mRNAs and the negative ferroptosis-related miRNAs.

and mRNAs that negatively correlated with ferroptosis. In addition, 33 pairs of miRNAs that negatively correlate with ferroptosis and mRNAs that positively correlate with ferroptosis were discovered.

After predicting the binding of miRNAs to lncRNAs, we were able to identify 11 pairs of miRNAs that were positively correlated with ferroptosis and lncRNAs that were negatively correlated with ferroptosis. Additionally, 13 pairs of miRNAs that were negatively correlated with ferroptosis and lncRNAs that were positively correlated with ferroptosis were found. After merging the aforementioned predictions, the ceRNA network focusing on miRNAs linked to ferroptosis either positively or negatively can be seen in **Figure 4A** and **4B**, correspondingly.

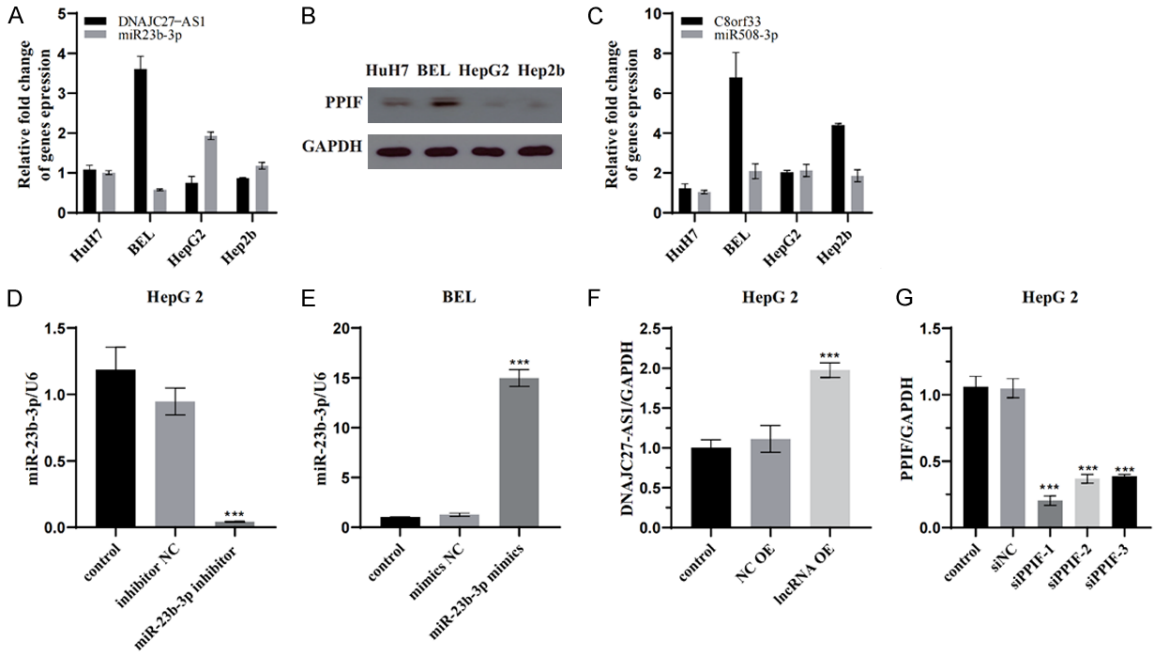

Figure 5. qPCR validation of plasmids and siRNAs in this study. A-C. Exploration of the transcriptional levels of some selected genes and the protein expression of PPIF in HuH7, BEL7402, HepG2, and Hep2b cells. D-G. Verification of the effectiveness of miR-23b-3p mimics, miR-23b-3p inhibitor, DNAJC27-AS1 overexpression plasmid, and siPPIF. BEL refers to the BEL7402 cell line. OE refers to overexpression. NC refers to negative control. ***P<0.001.

Verification of the DNAJC27-AS1/miR-23b-3p/PPIF ceRNA axis

To validate the credibility of the ferroptosis-related ceRNA network, we randomly selected two ceRNAs for experimental validation in the laboratory, namely DNAJC27-AS1/miR-23b-3p/PPIF and AC004988.1/miR-508-3p/C8orf33. Through qPCR verification, it was found that the expression levels of DNAJC27-AS1 and miR-23b-3p showed significant differences in the four human HCC cell lines. Therefore, we chose DNAJC27-AS1/miR-23b-3p/PPIF as the target for our validation experiments (**Figure 5A-C**). We subsequently constructed overexpression plasmids and siRNA for DNAJC27-AS1, miR-23b-3p, and PPIF, and confirmed their efficacy (**Figures 5D-G**, **6A**, **6E**).

Following the overexpression or interference with miR-23b-3p, the expressions of DNAJC27-AS1 and PPIF demonstrated opposite alterations. Similarly, interference with DNAJC27-AS1 resulted in decreased PPIF expression, while the overexpression of PPIF led to increased DNAJC27-AS1 expression (**Figure 6A-F**). The results from the dual luciferase reporter assay confirmed that miR-23b-3p directly interacts with PPIF and DNAJC27-AS1, and modulates their expression (**Figure 6G**, **6H**).

DNAJC27-AS1/miR-23b-3p/PPIF can regulate ferroptosis in HCC cells through a ceRNA mechanism

Knockdown of DNAJC27-AS1 expression elicited a concomitant decrease in GSH levels in BEL7402 cells, which could be restored by administration of Fer-1. Importantly, the GSH-protective effect of Fer-1 was nullified by both overexpression of PPIF and inhibition of miR-23b-3p. In line with these findings, miR-23b-3p mimics contributed to reduced GSH levels, which, nonetheless, could be rescued upon PPIF overexpression (**Figure 7A**). Encouragingly, we demonstrated that the DNAJC27-AS1 overexpression plasmid was capable of reinstating GSH levels in HepG2 cells upon Erastin-mediated depletion. Moreover, the observed increase in GSH levels due to DNAJC27-AS1 upregulation was blunted upon PPIF downregulation or miR-23b-3p upregulation (**Figure 7B**). CCK8 assays and ROS detection highlighted the cytoprotective roles of both DNAJC27-AS1 and PPIF in counteracting ROS-related cell damage, whereas miRNA exacerbated these

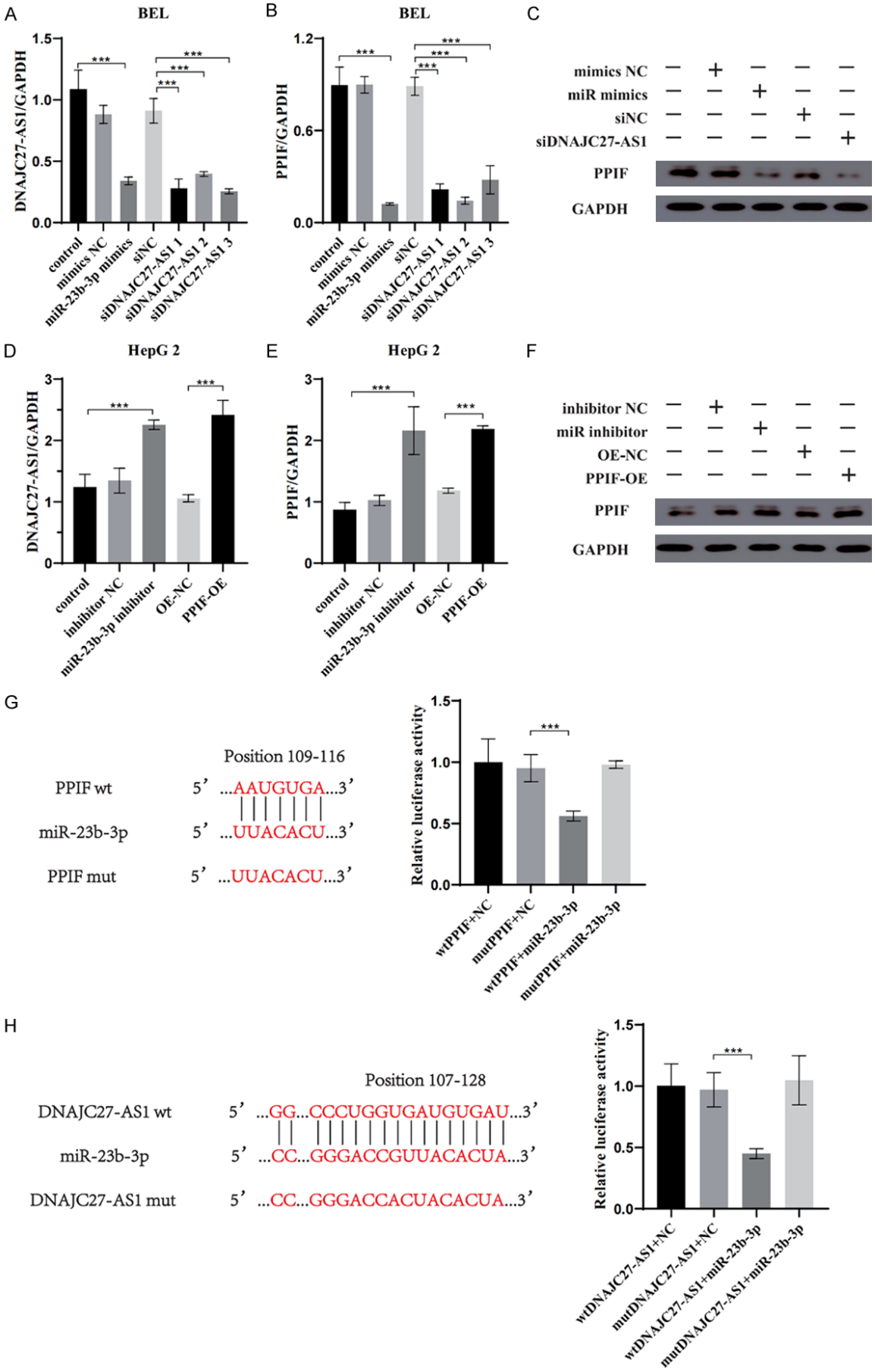
A
BEL
DNAJC27-AS1/GAPDH
control
mimics NC
miR-23b-3p mimics
siNC
siDNAJC27-AS1 1
siDNAJC27-AS1 2
siDNAJC27-AS1 3
B
BEL
PPIF/GAPDH
C
mimics NC
miR mimics
siNC
siDNAJC27-AS1
PPIF
GAPDH
D
HepG 2
DNAJC27-AS1/GAPDH
control
inhibitor NC
miR-23b-3p inhibitor
OE-NC
PPIF-OE
E
HepG 2
PPIF/GAPDH
F
inhibitor NC
miR inhibitor
OE-NC
PPIF-OE
PPIF
GAPDH
G
Position 109-116
PPIF wt 5' ...AAUGUGA...3'
miR-23b-3p 5' ...UUACACU...3'
PPIF mut 5' ...UUACACU...3'
Relative luciferase activity
wtPPIF+NC
mutPPIF+NC
wtPPIF+miR-23b-3p
mutPPIF+miR-23b-3p
H
Position 107-128
DNAJC27-AS1 wt 5' ...GG...CCCUGGUGAUGUGAU...3'
miR-23b-3p 5' ...CC...GGGACCGUUACACUA...3'
DNAJC27-AS1 mut 5' ...CC...GGGACCACUACACUA...3'
Relative luciferase activity
wtDNAJC27-AS1+NC
mutDNAJC27-AS1+NC
wtDNAJC27-AS1+miR-23b-3p
mutDNAJC27-AS1+miR-23b-3p

Figure 6. DNAJC27-AS1 and PPIF regulate each other's expression through direct interaction with miR-23b-3p. A. miR-23b-3p mimics can inhibit the transcription level of DNAJC27-AS1 and the efficiency verification of siDNAJC27-AS1. B, C. Both miR-23b-3p mimics and siDNAJC27-AS1 can inhibit the transcriptional level and the expression of PPIF. D. The miR-23b-3p inhibitor can elevate the transcriptional level of PPIF and the efficiency verification of the PPIF overexpression plasmid. E, F. Both miR-23b-3p inhibitor and PPIF overexpression can elevate the transcriptional level and the expression of DNAJC27-AS1. G. DNAJC27-AS1 and miR-23b-3p have direct interaction at positions 107 to 128 of DNAJC27-AS1. H. PPIF and miR-23b-3p have direct interaction at positions 109 to 116 of PPIF. OE refers to overexpression. BEL refers to the BEL7402 cell line. NC refers to negative control. Wt refers to the wild type. Mut refers to mutant. ***P<0.001.

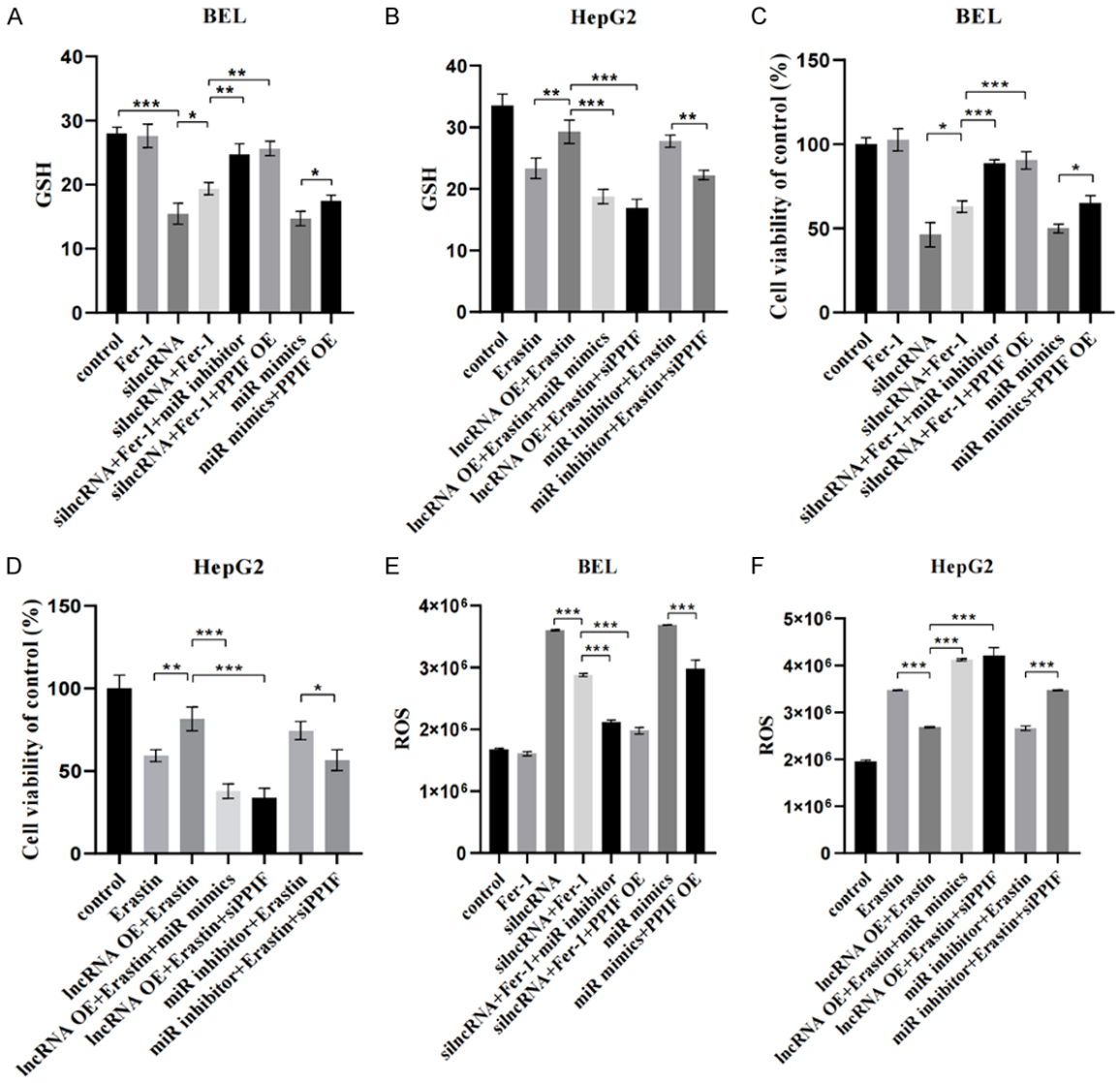

Figure 7. DNAJC27-AS1/miR-23b-3p/PPIF regulated ferroptosis in HCC cells. A. Detection of GSH content in BEL cells. B. Detection of GSH content in HepG2 cells. C. Cell viability assays in BEL cells. D. Cell viability assays in HepG2 cells. E. siDNAJC27-AS1 and miR-23b-3p mimic promote ROS production in BEL cells, while miR-23b-3p inhibitor and PPIF overexpression reduce ROS production. F. DNAJC27-AS1 overexpression reduces ROS production in HepG2 cells, while siPPIF promotes ROS production. LncRNA refers to DNAJC27-AS1. MiR refers to miR23b-3p. BEL refers to the BEL7402 cell line. OE refers to overexpression. *P<0.05, **P<0.01, ***P<0.001.

detrimental effects of ROS accumulation (**Figure 7C-F**).

The ferroptosis markers, namely GPX4, SLC7A11, and TP53, have confirmed the ability

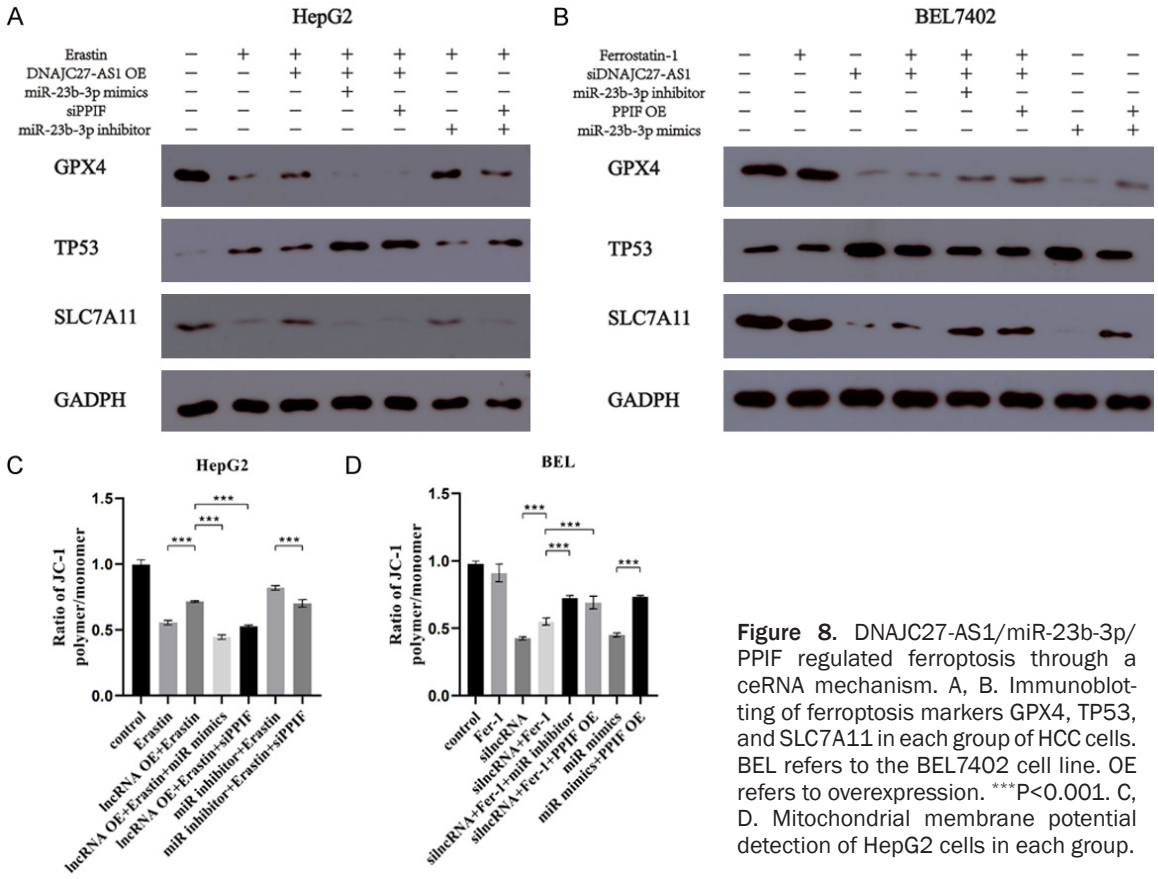

Figure 8. DNAJC27-AS1/miR-23b-3p/PPIF regulated ferroptosis through a ceRNA mechanism. A, B. Immunoblotting of ferroptosis markers GPX4, TP53, and SLC7A11 in each group of HCC cells. BEL refers to the BEL7402 cell line. OE refers to overexpression. ***P<0.001. C, D. Mitochondrial membrane potential detection of HepG2 cells in each group.

of the DNAJC27-AS1/miR-23b-3p/PPIF axis to regulate ferroptosis in HCC (**Figure 8A**, **8B**). Our findings indicated that DNAJC27-AS1 and PPIF can effectively restore the decreased mitochondrial membrane potential in HCC cells that has been induced by Erastin. Additionally, miR-23b-3p has been identified as an active inducer of mitochondrial membrane potential by modulating the expression levels of DNAJC27-AS1 and PPIF (**Figure 8C**, **8D**). The regulatory mechanism of the identified ceRNA axis on ferroptosis is illustrated in **Figure 9**.

Discussion

Hepatocellular carcinoma (HCC) ranks as the second most frequent cause of cancer-related death worldwide. It can evade established anti-cancer therapies [29]. Sorafenib, an FDA-approved drug for the systemic treatment of advanced HCC, has been shown to be susceptible to drug resistance. In this context, promoting ferroptosis may represent a promising strategy to overcome sorafenib resistance and enhance its therapeutic effectiveness. Recent studies have revealed a number of pathways and genes that are linked to ferroptosis and sorafenib resistance in HCC, such as TP53 mutant [30], Rb protein [31], and the p62-Keap1-Nrf2 pathway [32]. While we observed no significant differences in the scores of the ferroptosis gene set between cancerous and non-cancerous tissues, the association between ferroptosis and overall patient survival indicates its potential as a therapeutic target.

Many lncRNAs are closely associated with the occurrence and development of HCC. They may regulate HCC progression by ceRNA mechanisms. For example, the lncRNA MALAT1 has been shown to promote HCC migration and invasion through three ceRNA pathways: MALAT1/miR-30a-5p/Vimentin, MALAT1/miR-204/SIRT1, and MALAT1/miR-143-3p/ZEB1 [33-35]. Interestingly, the same lncRNA can mediate different phenotypes by interacting with different miRNAs. Another highly upregulated lncRNA in HCC is HULC, which affects the expression of CREB by sponging miR-372 to

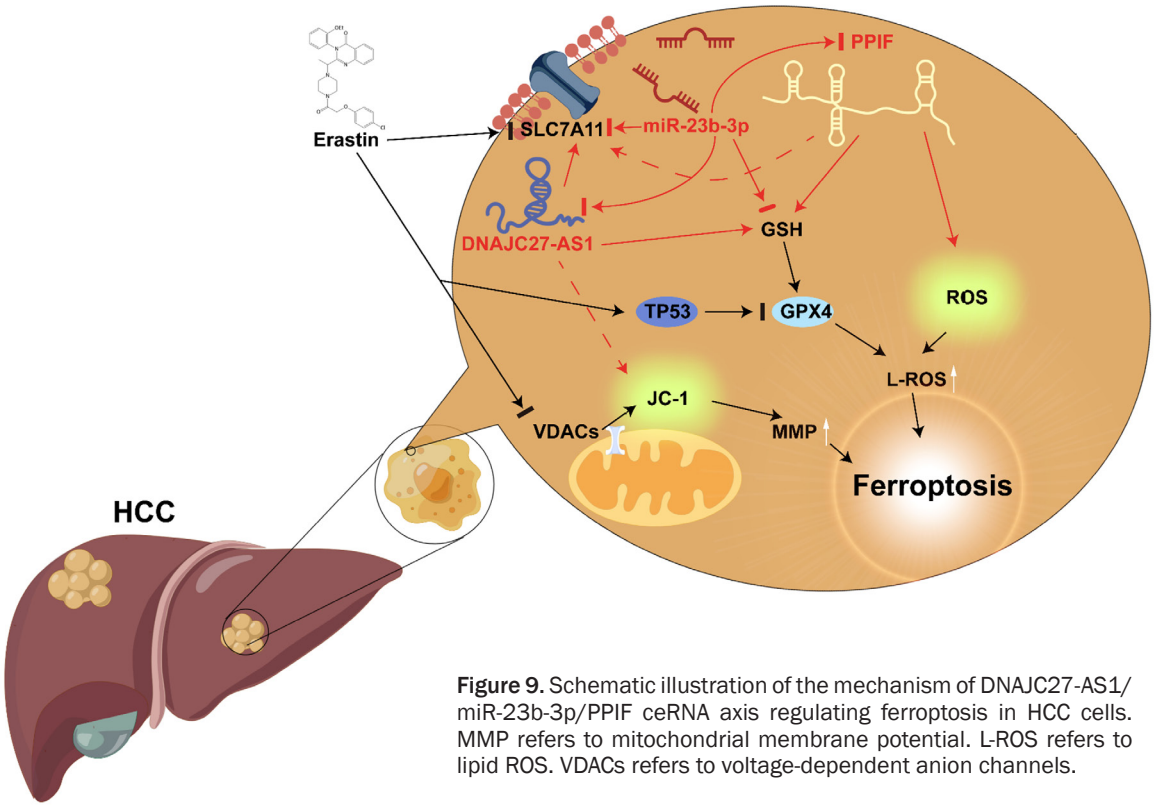

Figure 9. Schematic illustration of the mechanism of DNAJC27-AS1/miR-23b-3p/PPIF ceRNA axis regulating ferroptosis in HCC cells. MMP refers to mitochondrial membrane potential. L-ROS refers to lipid ROS. VDACs refers to voltage-dependent anion channels.

enhance chromatin accessibility and transcription [36]. HULC also increases ZEB1 expression by sponging miR-200a-3p, thereby accelerating the epithelial-mesenchymal transition of HCC cells [37]. Moreover, the HULC/USP22/SIRT1 pathway has been shown to weaken the chemosensitivity of HCC cells toward chemotherapeutic agents by acting as a protective autophagy ceRNA pathway [38]. We identified several modules that were most related to ferroptosis and constructed a ferroptosis-related ceRNA network in HCC. When multiple prediction software programs indicated the exact interaction between two RNAs, we incorporated this interaction into the network construction.

The gene encoding DNAJC27-AS1 is situated in the central region of the long arm of chromosome 2. A comprehensive investigation into open-angle glaucoma revealed that the bioprocess of DNAJC27-AS1 is enriched in regulating key cancer-associated and ferroptosis-related pathways, specifically the MAPK and Wnt pathways [39]. Our research confirms that DNAJC27-AS1 modulates the ferroptotic response in HCC cells, with overexpression of DNAJC27-AS1 leading to reduced cellular death induced by Erastin and decreased levels of ROS, while restoring the GSH levels that are typically reduced when Erastin is present. Furthermore, DNAJC27-AS1 directly interacts with miR-23b-3p to regulate the expression of its target gene, PPIF.

Previous studies have highlighted miR-23b-3p as an oncogene in HCC, with elevated levels predicting a poorer prognosis for patients [40]. It also was found that the level of circulating miR-23b-3p in the serum of HCC patients was significantly increased after sorafenib treatment [41]. SNGH16 and EGF1 regulate autophagy and sorafenib resistance in HCC cells through a ceRNA mechanism by regulating miR-23b-3p [42]. In addition, lncRNA HOTAIR increased the expression of ZEB1 by sponging miR-23b-3p, thereby promoting HCC invasion and metastasis [43]. However, to date, there is no comprehensive report on any correlation between miR-23b-3p and ferroptosis in HCC. Our study sheds light on this aspect and uncovers the intricate mechanisms underlying the regulation of HCC cell ferroptosis by miR-23b-3p through a ceRNA mode.

The PPIF gene encodes a protein that functions as a peptidyl-prolyl cis-trans isomerase, cata-

lyzing the isomerization of proline imine peptide bonds in oligopeptides and contributing to protein folding [44]. In this study, we have identified PPIF as a negative regulator of ferroptosis in liver cancer cells. Overexpression of PPIF can effectively rescue ferroptosis caused by DNAJC27-AS1 knockdown or miR-23b-3p mimics. Importantly, we have elucidated the regulatory role and the mechanism of the DNAJC27-AS1/miR-23b-3p/PPIF ceRNA axis in modulating ferroptosis in HCC.

Although this study is innovative in establishing a ferroptosis-associated ceRNA network in HCC, there are still some limitations that need to be addressed. First, the other ceRNA axes included in the constructed ceRNA network still need to be validated in future studies. Second, the experiments were carried out only in vitro, so further in vivo experiments and clinical trials are indispensable. Third, additional RNA interaction experiments are required to confirm the results.

Conclusion

In summary, our analysis has identified key lncRNAs, mRNAs, and miRNAs that are closely associated with ferroptosis in HCC. We have constructed a comprehensive ceRNA network incorporating these gene modules, which serves as a valuable resource for investigating the mechanisms of ferroptosis in HCC. Moreover, we have validated the significance of one of the ceRNA interactions in this network - the DNAJC27-AS1/miR-23b-3p/PPIF pathway - providing concrete evidence of the relevance of our findings. Our study might represent a step towards unlocking the mysteries of ferroptosis in HCC.

Disclosure of conflict of interest

None.

Address correspondence to: Yong Chen, Department of Hepatobiliary Surgery, The First Affiliated Hospital, Airforce Military Medical University, 169 Changle West Road, Xi'an 710032, Shaanxi, China. E-mail: gdwkcy@163.com

References

[1] Yang W, Ma Y, Liu Y, Smith-Warner SA, Simon TG, Chong DQ, Qi Q, Meyerhardt JA, Giovannucci EL, Chan AT and Zhang X. Association of intake of whole grains and dietary fiber with risk of hepatocellular carcinoma in US adults. JAMA Oncol 2019; 5: 879-886.

[2] Kwan SY, Sheel A, Song CQ, Zhang XO, Jiang T, Dang H, Cao Y, Ozata DM, Mou H, Yin H, Weng Z, Wang XW and Xue W. Depletion of TRRAP induces p53-independent senescence in liver cancer by down-regulating mitotic genes. Hepatology 2020; 71: 275-290.

[3] Zhu S, Zhang Q, Sun X, Zeh HJ 3rd, Lotze MT, Kang R and Tang D. HSPA5 regulates ferroptotic cell death in cancer cells. Cancer Res 2017; 77: 2064-2077.

[4] Koren E and Fuchs Y. Modes of regulated cell death in cancer. Cancer Discov 2021; 11: 245-265.

[5] Dixon SJ, Lemberg KM, Lamprecht MR, Skouta R, Zaitsev EM, Gleason CE, Patel DN, Bauer AJ, Cantley AM, Yang WS, Morrison B 3rd and Stockwell BR. Ferroptosis: an iron-dependent form of nonapoptotic cell death. Cell 2012; 149: 1060-1072.

[6] Yagoda N, von Rechenberg M, Zaganjor E, Bauer AJ, Yang WS, Fridman DJ, Wolpaw AJ, Smukste I, Peltier JM, Boniface JJ, Smith R, Lessnick SL, Sahasrabudhe S and Stockwell BR. RAS-RAF-MEK-dependent oxidative cell death involving voltage-dependent anion channels. Nature 2007; 447: 864-868.

[7] Chen PH, Wu J, Ding CC, Lin CC, Pan S, Bossa N, Xu Y, Yang WH, Mathey-Prevot B and Chi JT. Kinome screen of ferroptosis reveals a novel role of ATM in regulating iron metabolism. Cell Death Differ 2020; 27: 1008-1022.

[8] Yee PP, Wei Y, Kim SY, Lu T, Chih SY, Lawson C, Tang M, Liu Z, Anderson B, Thamburaj K, Young MM, Aregawi DG, Glantz MJ, Zacharia BE, Specht CS, Wang HG and Li W. Neutrophil-induced ferroptosis promotes tumor necrosis in glioblastoma progression. Nat Commun 2020; 11: 5424.

[9] Chu B, Kon N, Chen D, Li T, Liu T, Jiang L, Song S, Tavana O and Gu W. ALOX12 is required for p53-mediated tumour suppression through a distinct ferroptosis pathway. Nat Cell Biol 2019; 21: 579-591.

[10] Capelletti MM, Manceau H, Puy H and Peoc'h K. Ferroptosis in liver diseases: an overview. Int J Mol Sci 2020; 21: 4908.

[11] Du J, Wan Z, Wang C, Lu F, Wei M, Wang D and Hao Q. Designer exosomes for targeted and efficient ferroptosis induction in cancer via chemo-photodynamic therapy. Theranostics 2021; 11: 8185-8196.

[12] Sun X, Niu X, Chen R, He W, Chen D, Kang R and Tang D. Metallothionein-1G facilitates sorafenib resistance through inhibition of ferroptosis. Hepatology 2016; 64: 488-500.

[13] Gao R, Kalathur RKR, Coto-Llerena M, Ercan C, Buechel D, Shuang S, Piscuoglio S, Dill MT, Camargo FD, Christofori G and Tang F. YAP/TAZ

and ATF4 drive resistance to Sorafenib in hepatocellular carcinoma by preventing ferroptosis. EMBO Mol Med 2021; 13: e14351.
[14] Shi Y, Liu JB, Deng J, Zou DZ, Wu JJ, Cao YH, Yin J, Ma YS, Da F and Li W. The role of ceRNA-mediated diagnosis and therapy in hepatocellular carcinoma. Hereditas 2021; 158: 44.
[15] Wang H, Huo X, Yang XR, He J, Cheng L, Wang N, Deng X, Jin H, Wang N, Wang C, Zhao F, Fang J, Yao M, Fan J and Qin W. STAT3-mediated upregulation of lncRNA HOXD-AS1 as a ceRNA facilitates liver cancer metastasis by regulating SOX4. Mol Cancer 2017; 16: 136.
[16] Chen J, Yu Y, Li H, Hu Q, Chen X, He Y, Xue C, Ren F, Ren Z, Li J, Liu L, Duan Z, Cui G and Sun R. Long non-coding RNA PVT1 promotes tumor progression by regulating the miR-143/HK2 axis in gallbladder cancer. Mol Cancer 2019; 18: 33.
[17] Qi W, Li Z, Xia L, Dai J, Zhang Q, Wu C and Xu S. LncRNA GABPB1-AS1 and GABPB1 regulate oxidative stress during erastin-induced ferroptosis in HepG2 hepatocellular carcinoma cells. Sci Rep 2019; 9: 16185.
[18] Zhang Y, Luo M, Cui X, O'Connell D and Yang Y. Long noncoding RNA NEAT1 promotes ferroptosis by modulating the miR-362-3p/MIOX axis as a ceRNA. Cell Death Differ 2022; 29: 1850-1863.
[19] Mao C, Wang X, Liu Y, Wang M, Yan B, Jiang Y, Shi Y, Shen Y, Liu X, Lai W, Yang R, Xiao D, Cheng Y, Liu S, Zhou H, Cao Y, Yu W, Muegge K, Yu H and Tao Y. A G3BP1-interacting lncRNA promotes ferroptosis and apoptosis in cancer via nuclear sequestration of p53. Cancer Res 2018; 78: 3484-3496.
[20] Ye Y, Dai Q and Qi H. A novel defined pyroptosis-related gene signature for predicting the prognosis of ovarian cancer. Cell Death Discov 2021; 7: 71.
[21] Wan RJ, Peng W, Xia QX, Zhou HH and Mao XY. Ferroptosis-related gene signature predicts prognosis and immunotherapy in glioma. CNS Neurosci Ther 2021; 27: 973-986.
[22] Vejnar CE, Blum M and Zdobnov EM. miRmap web: comprehensive microRNA target prediction online. Nucleic Acids Res 2013; 41: W165-168.
[23] Miranda KC, Huynh T, Tay Y, Ang YS, Tam WL, Thomson AM, Lim B and Rigoutsos I. A pattern-based method for the identification of MicroRNA binding sites and their corresponding heteroduplexes. Cell 2006; 126: 1203-1217.
[24] Wong N and Wang X. miRDB: an online resource for microRNA target prediction and functional annotations. Nucleic Acids Res 2015; 43: D146-152.
[25] Nielsen CB, Shomron N, Sandberg R, Hornstein E, Kitzman J and Burge CB. Determinants of targeting by endogenous and exogenous microRNAs and siRNAs. RNA 2007; 13: 1894-1910.
[26] Huang HY, Lin YC, Li J, Huang KY, Shrestha S, Hong HC, Tang Y, Chen YG, Jin CN, Yu Y, Xu JT, Li YM, Cai XX, Zhou ZY, Chen XH, Pei YY, Hu L, Su JJ, Cui SD, Wang F, Xie YY, Ding SY, Luo MF, Chou CH, Chang NW, Chen KW, Cheng YH, Wan XH, Hsu WL, Lee TY, Wei FX and Huang HD. miRTarBase 2020: updates to the experimentally validated microRNA-target interaction database. Nucleic Acids Res 2020; 48: D148-D154.
[27] Jeggari A, Marks DS and Larsson E. miRcode: a map of putative microRNA target sites in the long non-coding transcriptome. Bioinformatics 2012; 28: 2062-2063.
[28] Li JH, Liu S, Zhou H, Qu LH and Yang JH. starBase v2.0: decoding miRNA-ceRNA, miRNA-ncRNA and protein-RNA interaction networks from large-scale CLIP-Seq data. Nucleic Acids Res 2014; 42: D92-97.
[29] Cancer Genome Atlas Research Network. Electronic address: wheeler@bcm.edu; Cancer Genome Atlas Research Network. Comprehensive and integrative genomic characterization of hepatocellular carcinoma. Cell 2017; 169: 1327-1341, e1323.
[30] Jennis M, Kung CP, Basu S, Budina-Kolomets A, Leu JI, Khaku S, Scott JP, Cai KQ, Campbell MR, Porter DK, Wang X, Bell DA, Li X, Garlick DS, Liu Q, Hollstein M, George DL and Murphy ME. An African-specific polymorphism in the TP53 gene impairs p53 tumor suppressor function in a mouse model. Genes Dev 2016; 30: 918-930.
[31] Louandre C, Marcq I, Bouhlal H, Lachaier E, Godin C, Saidak Z, Francois C, Chatelain D, Debuysscher V, Barbare JC, Chauffert B and Galmiche A. The retinoblastoma (Rb) protein regulates ferroptosis induced by sorafenib in human hepatocellular carcinoma cells. Cancer Lett 2015; 356: 971-977.
[32] Yu J and Wang JQ. Research mechanisms of and pharmaceutical treatments for ferroptosis in liver diseases. Biochimie 2021; 180: 149-157.
[33] Chen L, Yao H, Wang K and Liu X. Long non-coding RNA MALAT1 regulates ZEB1 expression by sponging miR-143-3p and promotes hepatocellular carcinoma progression. J Cell Biochem 2017; 118: 4836-4843.
[34] Hou Z, Xu X, Zhou L, Fu X, Tao S, Zhou J, Tan D and Liu S. The long non-coding RNA MALAT1 promotes the migration and invasion of hepatocellular carcinoma by sponging miR-204 and releasing SIRT1. Tumour Biol 2017; 39: 1010428317718135.
[35] Pan Y, Tong S, Cui R, Fan J, Liu C, Lin Y, Tang J, Xie H, Lin P, Zheng T and Yu X. Long non-coding MALAT1 functions as a competing endogenous

RNA to regulate vimentin expression by sponging miR-30a-5p in hepatocellular carcinoma. Cell Physiol Biochem 2018; 50: 108-120.
[36] Wang J, Liu X, Wu H, Ni P, Gu Z, Qiao Y, Chen N, Sun F and Fan Q. CREB up-regulates long non-coding RNA, HULC expression through interaction with microRNA-372 in liver cancer. Nucleic Acids Res 2010; 38: 5366-5383.
[37] Li SP, Xu HX, Yu Y, He JD, Wang Z, Xu YJ, Wang CY, Zhang HM, Zhang RX, Zhang JJ, Yao Z and Shen ZY. LncRNA HULC enhances epithelial-mesenchymal transition to promote tumorigenesis and metastasis of hepatocellular carcinoma via the miR-200a-3p/ZEB1 signaling pathway. Oncotarget 2016; 7: 42431-42446.
[38] Xiong H, Ni Z, He J, Jiang S, Li X, He J, Gong W, Zheng L, Chen S, Li B, Zhang N, Lyu X, Huang G, Chen B, Zhang Y and He F. LncRNA HULC triggers autophagy via stabilizing Sirt1 and attenuates the chemosensitivity of HCC cells. Oncogene 2017; 36: 3528-3540.
[39] Zhou M, Lu B, Tan W and Fu M. Identification of lncRNA-miRNA-mRNA regulatory network associated with primary open angle glaucoma. BMC Ophthalmol 2020; 20: 104.
[40] Hayashi M, Yamada S, Kurimoto K, Tanabe H, Hirabayashi S, Sonohara F, Inokawa Y, Takami H, Kanda M, Tanaka C, Nakayama G, Koike M and Kodera Y. miR-23b-3p plays an oncogenic role in hepatocellular carcinoma. Ann Surg Oncol 2021; 28: 3416-3426.
[41] Manganelli M, Grossi I, Ferracin M, Guerriero P, Negrini M, Ghidini M, Senti C, Ratti M, Pizzo C, Passalacqua R, Molfino S, Baiocchi G, Portolani N, Marchina E, De Petro G and Salvi A. Longitudinal circulating levels of miR-23b-3p, miR-126-3p and lncRNA GAS5 in HCC patients treated with Sorafenib. Biomedicines 2021; 9: 813.
[42] Jing Z, Ye X, Ma X, Hu X, Yang W, Shi J, Chen G and Gong L. SNGH16 regulates cell autophagy to promote Sorafenib resistance through suppressing miR-23b-3p via sponging EGR1 in hepatocellular carcinoma. Cancer Med 2020; 9: 4324-4338.
[43] Yang T, He X, Chen A, Tan K and Du X. LncRNA HOTAIR contributes to the malignancy of hepatocellular carcinoma by enhancing epithelial-mesenchymal transition via sponging miR-23b-3p from ZEB1. Gene 2018; 670: 114-122.
[44] Davis TL, Walker JR, Campagna-Slater V, Finerty PJ, Paramanathan R, Bernstein G, MacKenzie F, Tempel W, Ouyang H, Lee WH, Eisenmesser EZ and Dhe-Paganon S. Structural and biochemical characterization of the human cyclophilin family of peptidyl-prolyl isomerases. PLoS Biol 2010; 8: e1000439.